


Generation and control of optical frequency combs using cavity electromagnetically induced transparency

Jiahua Li,^{1,*} Ye Qu,¹ Rong Yu,² and Ying Wu^{1,†}

¹*School of Physics, Huazhong University of Science and Technology, Wuhan 430074, People's Republic of China*

²*School of Science, Wuhan Institute of Technology, Wuhan 430205, People's Republic of China*

 (Received 5 December 2017; revised manuscript received 31 January 2018; published 15 February 2018)

We explore theoretically the generation and all-optical control of optical frequency combs (OFCs) in photon transmission based on a combination of single-atom-cavity quantum electrodynamics (CQED) and electromagnetically induced transparency (EIT). Here an external control field is used to form the cavity dark mode of the CQED system. When the strengths of the applied EIT control field are appropriately tuned, enhanced comb generation can be achieved. We discuss the properties of the dark mode and clearly show that the formation of the dark mode enables the efficient generation of OFCs. In our approach, the comb spacing is determined by the beating frequency between the driving pump and seed lasers. Our demonstrated theory may pave the way towards all-optical coherent control of OFCs using a CQED architecture.

DOI: [10.1103/PhysRevA.97.023826](https://doi.org/10.1103/PhysRevA.97.023826)

I. INTRODUCTION

The optical frequency comb (OFC) spectrum [1–4] consists of a series of equally spaced teeth with fixed frequency positions $f_m = f_0 + mf_{\text{rep}}$, where m is an integer, f_0 the carrier frequency offset, and f_{rep} the laser repetition rate. Typically, the frequency difference between neighboring teeth f_{rep} is on the order of 10 MHz to 1 GHz. A broad range of techniques has been developed for generating the OFC spectrum. Traditionally, OFCs with a stable repetition rate can be generated in nonlinear optical fibers by utilizing mode-locking lasers [1,2]. In recent years, much attention has been focused on the generation of OFCs based on parametric frequency conversion compact optical microresonators [3–7]. However, these methods typically either need high optical pump power to obtain a larger number of comb lines due to large insertion losses or limit comb spacing tunability in unchanged Kerr materials. It appears more favorable and desired for practical applications to generate OFCs with ultralow operating power and tunable comb-tooth spacing. The goal of this paper is to generate an OFC spectrum with low input powers and a tunable slow repetition rate using the four-wave-mixing processes induced by electromagnetically induced transparency (EIT) with an atom in a high-finesse optical cavity.

Coherently driven, three-level Λ -type atoms or comparable solid-state emitters, instead of two-level atoms, are widely used to study a variety of new quantum optical phenomena in which the dynamics of a reference probe beam can be efficiently controlled by a secondary control beam. One of the most important aspects is the modification of the absorption, dispersion, and nonlinearity of the system due to quantum coherence and interference. Examples include EIT [8–11] and

related topics [12–14]. Over the past few years, several groups have succeeded in trapping and demonstrating EIT of single-particle systems in free space [15–17]. Compared to particles in free space, the introduction of an optical cavity has several major advantages since it can enhance the light-atom coupling in the setup and also effectively increases the nonlinearity of the studied system. Furthermore, an optical cavity is also useful for controlling the mode structure, thereby enabling high input-output efficiencies. Optical control has already been realized in single-particle cavity quantum electrodynamics (CQED) experiments [18–26]. Incorporating EIT technique can boost the capabilities of CQED. It has been shown that merging EIT with CQED and a single quantum of matter is likely to become the cornerstone for many novel applications [27–35].

Recently, Mücke *et al.* experimentally observed EIT with a single rubidium atom trapped inside a high-finesse optical cavity, where the atom serves as a quantum-optical transistor with the ability to coherently control the transmission of light through the cavity [28]. Based on this achievement, in the present work we put forward a single-atom-cavity EIT scheme to generate and control OFCs at driving laser powers as low as a few nanowatts by means of a classical control field. When the strengths of the control field are appropriately tuned, enhanced OFC generation can be achieved by using state-of-the-art experimental parameters of the CQED systems. The comb-tooth spacing can be well tuned by changing the beating frequency between the driving pump and seed lasers. A few-megahertz repetition rate can be achieved, which is small for any microcomb. This is otherwise possible in the standard OFC only by changing the physical cavity length. In addition to numerical simulations demonstrating this controlled OFC effect, a complete physical explanation of the underlying mechanism is presented. The proposed scheme would be applicable to several other types of optical cavity systems (e.g., photonic crystal cavities, pillar cavities, microtoroids, and bottle microresonators) [26,36,37]. The scheme in prin-

*huajia_li@163.com

†yingwu2@126.com

principle is also suitable for a multiatom CQED system (i.e., an ensemble of atoms inside a high-finesse optical cavity) [38–40].

The organization of the paper is as follows. In Sec. II we establish the theoretical model and present the Hamiltonian of the system within a rotating frame as well as the Heisenberg-Langevin equations of motion. Then we choose the readily achievable atom-cavity system parameters. In Sec. III we illustrate the generation and control of OFCs based on a combination of single-atom CQED and EIT in the transmission power spectra via numerical simulations. Also, we discuss the underlying physical mechanism of these phenomena. Finally, in Sec. IV a brief summary and conclusions are given.

II. SYSTEM

We consider a single atom with three energy levels in a Λ configuration [see Figs. 1(a) and 1(b)] coupled to a single electromagnetic mode of a high-finesse optical resonator and an externally classical control laser. Details of this cavity EIT device in the regime of a single atom have been experimentally reported and demonstrated in Refs. [28–32]. It should be pointed out that the three-level atom, as modeled here, is a simplified three-level quantum system, which can be a nitrogen-vacancy center [41], a quantum dot [42,43], a superconducting qubit [44,45], or a genuine atom [28–32]. Notice that, for the different three-level quantum emitters

mentioned above, the values of the system parameters exhibit a significantly large difference or gap. So, for the convenience of the parameter choice, we take into account a specific ^{87}Rb atom [28–32].

As illustrated in Ref. [28], the relevant electronic levels of the ^{87}Rb atom (nuclear spin $I = 3/2$) are the long-lived hyperfine ground states $|1\rangle = |5^2S_{1/2}, F = 1\rangle$ and $|2\rangle = |5^2S_{1/2}, F = 2\rangle$, which couple to the common excited state $|3\rangle = |5^2P_{3/2}, F = 1\rangle$ via an external continuous-wave (cw) control laser propagating along the y direction and the quantum cavity mode along the z direction, respectively. This is the so-called cavity EIT configuration. This forms a Λ -level scheme suitable for the generation of a coherent dark state [10]. Specifically, the cavity field with resonance frequency ω_a and vacuum Rabi frequency (coupling constant) g_a interacts with the $|1\rangle \leftrightarrow |3\rangle$ transition of a three-level Λ -type atom. Here $g_a = \mu_{31}\sqrt{\omega_a/2\hbar\epsilon_0 V}$, where μ_{31} is the atomic transition dipole moment for the cavity-field coupling, $|1\rangle \leftrightarrow |3\rangle$, and V is the cavity-mode volume. At the same time, the cw control laser, defined as $E_c(t) = \mathcal{E}_c e^{-i\omega_c t}$ with the angular frequency ω_c and the field strength \mathcal{E}_c , drives the atomic transition $|2\rangle \leftrightarrow |3\rangle$. The cavity is coherently driven by a biharmonic cw laser composed of a pump field and a seed field, i.e., $S_{\text{dr}}(t) = \mathcal{E}_p e^{-i\omega_p t} + \mathcal{E}_s e^{-i\omega_s t}$, where ω_j ($j = p, s$) is the angular frequency and \mathcal{E}_j are the strengths of the biharmonic driving components with power $P_j = \hbar\omega_j \mathcal{E}_j^2$ incident on the optical cavity with field decay rate κ_a . Introducing the electric dipole and rotating-wave approximations, the time-independent Hamiltonian describing the dynamics of such a coupled atom-cavity system driven by a biharmonic laser field is given in a rotating frame by [11,31] $\hat{\mathcal{H}}/\hbar = \Delta_p \hat{a}^\dagger \hat{a} + (\Delta_p + \Delta_a - \Delta_c) \hat{\sigma}_{22} + (\Delta_p + \Delta_a) \hat{\sigma}_{33} + (\Omega_c \hat{\sigma}_{32} + \text{H.c.}) + (g_a \hat{a} \hat{\sigma}_{31} + \text{H.c.}) + \sqrt{\kappa_a} (\mathcal{E}_p \hat{a}^\dagger + \mathcal{E}_s e^{-i\Delta t} \hat{a}^\dagger + \text{H.c.})$, where \hat{a} and \hat{a}^\dagger are photon annihilation and creation operators, respectively, and $\hat{\sigma}_{ij} = |i\rangle\langle j|$, $i, j = 1, 2, 3$, are the atomic raising and lowering operators ($i \neq j$) and the atomic energy-level population operators ($i = j$), respectively. The energy of the ground state $|1\rangle$ is set as zero (i.e., $\hbar\omega_1 = 0$) for simplicity. Here Ω_c is the classical Rabi frequency of the control laser and is given by $\Omega_c = \mu_{32} \mathcal{E}_c / 2\hbar$, where μ_{32} is the dipole moment of the atomic transition being driven by the control laser. In addition, $\Delta_p = \omega_a - \omega_p$ is the detuning of the cavity resonance frequency ω_a from the frequency of the pump component ω_p , $\Delta_a = \omega_{31} - \omega_a$ is the detuning of the $|1\rangle \leftrightarrow |3\rangle$ transition frequency ω_{31} from the cavity resonance frequency ω_a , and $\Delta_c = \omega_{32} - \omega_c$ is the detuning of the $|2\rangle \leftrightarrow |3\rangle$ transition frequency ω_{32} from the control-field frequency ω_c . Further, $\Delta = \omega_s - \omega_p$ is the beating frequency between the seed field ω_s and the pump field ω_p for the biharmonic driving. Without loss of generality, we take Rabi frequencies g_a and Ω_c to be real in the following.

To fully describe the CQED system, losses need to be introduced phenomenologically. The two main loss mechanisms are the cavity-field decay rate $\kappa_a = \omega_a/Q$ (where Q is the quality factor of the optical cavity) and the atomic polarization decay rates γ_{31} and γ_{32} from the excited level $|3\rangle$ to the levels $|1\rangle$ and $|2\rangle$, respectively. The relaxation rate of coherence among the levels $|1\rangle$ and $|2\rangle$ is negligible and can be safely neglected because this transition is non-dipole-allowed in our considered

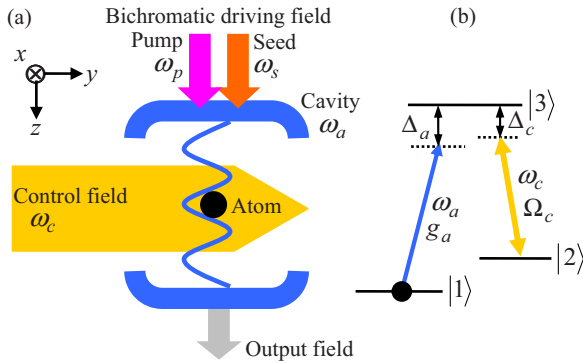


FIG. 1. (a) Illustration of the setup. A single rubidium atom is trapped inside a high-finesse optical cavity and illuminated by a control laser along the y axis. The cavity considered here can be symmetric; the loss rates of the two cavity mirrors are the same. The blue curve denotes the atom-cavity coupling strength along the z axis. A biharmonic cw driving laser consisting of a pump field and a seed field is coupled into the cavity mode along the cavity axis and its transmission can be measured using an optical spectrum analyzer to infer the key features of the cavity EIT system. (b) Atomic level scheme of the ^{87}Rb D_2 line with relevant transitions ($|1\rangle = |5^2S_{1/2}, F = 1\rangle$, $|2\rangle = |5^2S_{1/2}, F = 2\rangle$, and $|3\rangle = |5^2P_{3/2}, F = 1\rangle$). A three-level atom in the Λ configuration interacts with a cavity mode (angular frequency ω_a , vacuum Rabi frequency g_a , and frequency detuning Δ_a) from the atomic $|1\rangle \leftrightarrow |2\rangle$ transition (transition frequency ω_{31}) and an external control laser (angular frequency ω_c , Rabi frequency Ω_c , and frequency detuning Δ_c) from the atomic $|2\rangle \leftrightarrow |3\rangle$ transition (transition frequency ω_{32}), respectively. The three-level atom is initially in the ground state $|1\rangle$.

model. With this notation, the dynamics of a coupled atom-cavity system can be described by the Heisenberg-Langevin equations of motion as

$$\frac{d\hat{a}}{dt} = -(i\Delta_p + \kappa_a)\hat{a} - ig_a\hat{\sigma}_{13} - i\sqrt{\kappa_a}(\mathcal{E}_p + \mathcal{E}_s e^{-i\Delta t}) + \hat{h}_a, \quad (1)$$

$$\frac{d\hat{\sigma}_{11}}{dt} = 2\gamma_{31}\hat{\sigma}_{33} + ig_a\hat{a}\hat{\sigma}_{31} - ig_a\hat{a}^\dagger\hat{\sigma}_{13} + \hat{h}_{11}, \quad (2)$$

$$\frac{d\hat{\sigma}_{22}}{dt} = 2\gamma_{32}\hat{\sigma}_{33} + i\Omega_c\hat{\sigma}_{32} - i\Omega_c\hat{\sigma}_{23} + \hat{h}_{22}, \quad (3)$$

$$\frac{d\hat{\sigma}_{12}}{dt} = -i(\Delta_p + \Delta_a - \Delta_c)\hat{\sigma}_{12} - i\Omega_c\hat{\sigma}_{13} + ig_a\hat{a}\hat{\sigma}_{32} + \hat{h}_{12}, \quad (4)$$

$$\frac{d\hat{\sigma}_{13}}{dt} = -[i(\Delta_p + \Delta_a) + \gamma_{31} + \gamma_{32}]\hat{\sigma}_{13} - i\Omega_c\hat{\sigma}_{12} + ig_a\hat{a}(\hat{\sigma}_{33} - \hat{\sigma}_{11}) + \hat{h}_{13}, \quad (5)$$

$$\frac{d\hat{\sigma}_{23}}{dt} = -(i\Delta_c + \gamma_{31} + \gamma_{32})\hat{\sigma}_{23} - ig_a\hat{a}\hat{\sigma}_{21} + i\Omega_c(\hat{\sigma}_{33} - \hat{\sigma}_{22}) + \hat{h}_{23}, \quad (6)$$

with $\hat{\sigma}_{11} + \hat{\sigma}_{22} + \hat{\sigma}_{33} = 1$. The operators \hat{h}_a , \hat{h}_{11} , \hat{h}_{22} , \hat{h}_{12} , \hat{h}_{13} , and \hat{h}_{23} above are the noise operators that conserve the commutation relations at all times. The Langevin noise operators have zero mean values by assumption in this treatment, as shown already in earlier works [46,47]. Equation (1) describes the dynamics of the cavity modes in the optical cavity. Equations (2)–(6) describe the dynamics of the three-level Λ -type atom. Optical emission from the cavity mode is directly proportional to the corresponding intracavity photon number $\langle \hat{a}^\dagger(t)\hat{a}(t) \rangle$ [23,24,48], where $\langle \cdot \rangle$ stands for the expectation value. In the work of Dong *et al.* [48], these spectra are also called intracavity emission spectra and below we will present the numerical results for the transmission response [i.e., the cavity-output power $\hbar\omega_a\kappa_a\langle \hat{a}^\dagger(t)\hat{a}(t) \rangle$] in the frequency domain.

In the following discussion, we consider that the optical cavity operates in the intermediate-coupling regime with the experiment parameters $\{g_a, \kappa_a, \gamma_{31}, \gamma_{32}\}/2\pi = \{4.5, 2.9, 3, 3\}$ MHz from Ref. [28]. The wavelength of the driving pump laser is chosen to be 780 nm. When the amplitudes of the pump and seed fields are set as $\mathcal{E}_p = \mathcal{E}_s = 10^5 \sqrt{\text{Hz}}$, the corresponding powers are $P_p = P_s = 2.5$ nW according to the expression $P_j = \hbar\omega_j\mathcal{E}_j^2$ ($j = p, s$). For the cavity with the length $L = 495 \mu\text{m}$ [28], it has a high finesse of $\mathcal{F} = 5.2 \times 10^4$ based on the formula $\mathcal{F} = \pi c/L\kappa$ and has a large bandwidth of $\Delta\omega/2\pi = 7.4$ GHz based on the formula $\Delta\omega = \omega_a/\mathcal{F}$, where c is the speed of light. Outside this bandwidth of the cavity, no modes are allowed and therefore it is the fundamental bandwidth limit of the achievable OFC in the proposed scheme. In the following, all the generated OFC spectra are located within the bandwidth of the optical cavity.

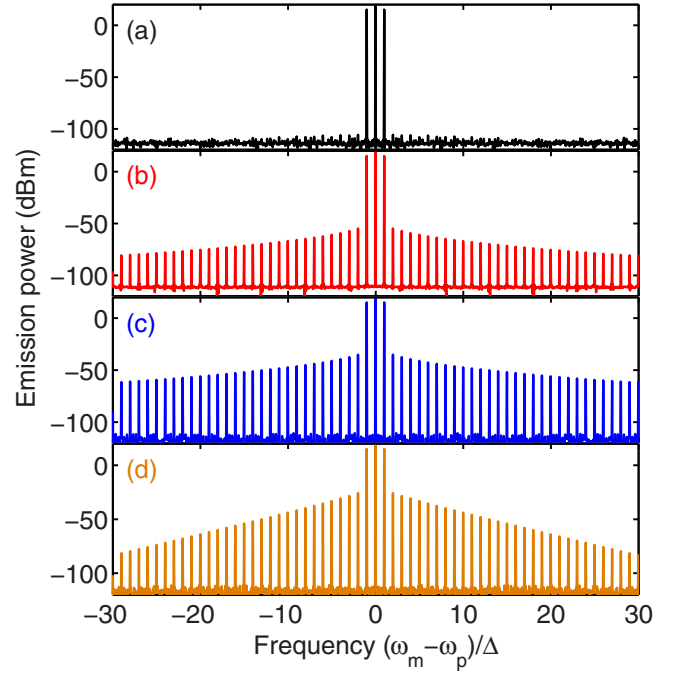


FIG. 2. The OFC spectra generated in the cavity EIT system for four different values of the control laser Ω_c at $P_p = P_s = 2.5$ nW and $\Delta/2\pi = 1$ MHz: (a) $\Omega_c/2\pi = 0$ MHz, (b) $\Omega_c/2\pi = 0.8$ MHz, (c) $\Omega_c/2\pi = 8$ MHz, and (d) $\Omega_c/2\pi = 80$ MHz. Here we only consider the case of resonant excitations for the pump, control, and cavity fields, in which the cavity EIT effect is the most prominent. For the case of nonresonant excitations, the powers of the comb teeth decrease with increasing detunings (not shown here). The other system parameters for the simulation are $g_a/2\pi = 4.5$ MHz, $\kappa_a/2\pi = 2.9$ MHz, and $\gamma_{31}/2\pi = \gamma_{32}/2\pi = 3$ MHz.

III. NUMERICAL SIMULATIONS AND DISCUSSION

Figure 2 shows how the considered cavity-EIT system can be used to coherently modify the OFC spectra of photon emission. As can be seen in Fig. 2, the applied EIT control field affects significantly the magnitude of the respective comb teeth in the generated OFC spectra. Specifically, for the case that the control laser is switched off [i.e., $\Omega_c/2\pi = 0$ MHz in Fig. 2(a)], the phenomenon of optical high-order comb teeth cannot be generated efficiently because the intracavity dark state is absent. Under this condition, the nonlinear optical process of parametric frequency conversion is very weak and the generated high-order comb teeth are almost absorbed. More specifically from Fig. 2(a), the rightmost comb line at $(\omega_1 - \omega_p)/\Delta = 1$ just represents the seed field $\omega_s \equiv \omega_1$. The central comb line at $(\omega_0 - \omega_p)/\Delta = 0$ happens to be the pump field $\omega_p \equiv \omega_0$. The leftmost comb line at $(\omega_{-1} - \omega_p)/\Delta = -1$ stands for the idler field ω_{-1} . For more details about these three comb lines (see also Fig. 4 below).

In contrast, when the control laser is switched on for $\Omega_c/2\pi = 0.8$ MHz in Fig. 2(b), a series of higher-order comb teeth can be observed in the photon emission spectra, which is a signature that the system is driven toward a dark mode. As the sideband order is increased, the intensity of the higher-order comb tooth is decreased gradually. The frequency of the comb tooth of order m can be formulated by the relationship

$\omega_m = \omega_p + m\Delta$, where m is the number of comb teeth, $m = 0$ corresponds to the pump field ω_p , $m = 1$ corresponds to the seed field $\omega_s = \omega_p + \Delta$, and $m = -1$ corresponds to the idler field $\omega_{-1} = \omega_p - \Delta$. These equidistant comb teeth will be explained below in detail. When $\Omega_c/2\pi = 8$ MHz in Fig. 2(c), the intensity of each comb tooth is largely enhanced. However, for the case that $\Omega_c/2\pi = 80$ MHz in Fig. 2(d), the intensity of the comb tooth quickly decreases with the order of the comb tooth.

Figure 3(a) displays the dependences of the picked 5th, 15th, and 25th comb-tooth intensities from Fig. 2 on the control field Ω_c to quantify the above observation further. These comb-tooth intensities first increase with the control field and then decrease gradually. The results also provide more support to the claims that this method can be used to suppress or enhance the intensities of the comb lines. To gain insight into the origin of the change of the comb-tooth intensity, we define two cavity polariton modes according to Ref. [10]: a dark-state polariton mode $\hat{A}_{ds} = \cos\theta\hat{a} - \sin\theta\hat{\sigma}_{12}$ and a bright-state polariton mode $\hat{A}_{bs} = \sin\theta\hat{a} + \cos\theta\hat{\sigma}_{12}$, with $\sin\theta = g_a(g_a^2 + \Omega_c^2)^{-1/2}$ and $\cos\theta = \Omega_c(g_a^2 + \Omega_c^2)^{-1/2}$, respectively. In order to demonstrate the fact that the dark-mode formation can enable efficient generation of OFCs in the cavity EIT system, we introduce the dark-mode fraction, which is defined as the ratio of the dark-mode population over the total bright-mode and dark-mode population, i.e., $\eta = \langle \hat{A}_{ds}^\dagger \hat{A}_{ds} \rangle / (\langle \hat{A}_{ds}^\dagger \hat{A}_{ds} \rangle + \langle \hat{A}_{bs}^\dagger \hat{A}_{bs} \rangle)$. Figure 3(b) plots the calculated dark-mode fraction η as a function of Ω_c . Here η is large and correspondingly the optical high-order comb-tooth intensity of photon emission from the cavity mode is high. However, after the system is driven into a predominantly

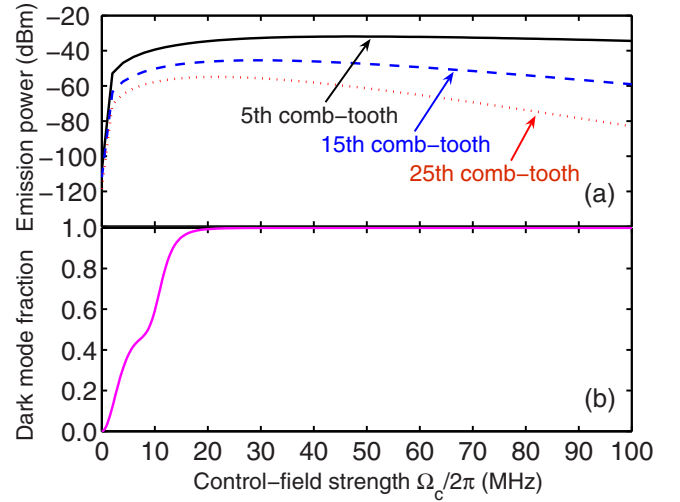


FIG. 3. (a) The 5th, 15th, and 25th comb-tooth intensities from Fig. 2 versus the control-field strength Ω_c . (b) Calculated dark-mode fraction η . The other parameters are the same as in Fig. 2.

dark mode, a further increase in Ω_c leads to a saturation and then a decrease in the emission. In other words, the physics behind such atom-cavity-assisted OFC generation is due to the formation of the intracavity dark state.

In what follows, we further give the physical explanations of the comb-tooth spacing and linewidth in the generated OFC spectra. In an optical cavity EIT system with appropriate dispersion, an external biharmonic cw driving resource consisting of a pump field ω_p and a seed field ω_s , which is launched into

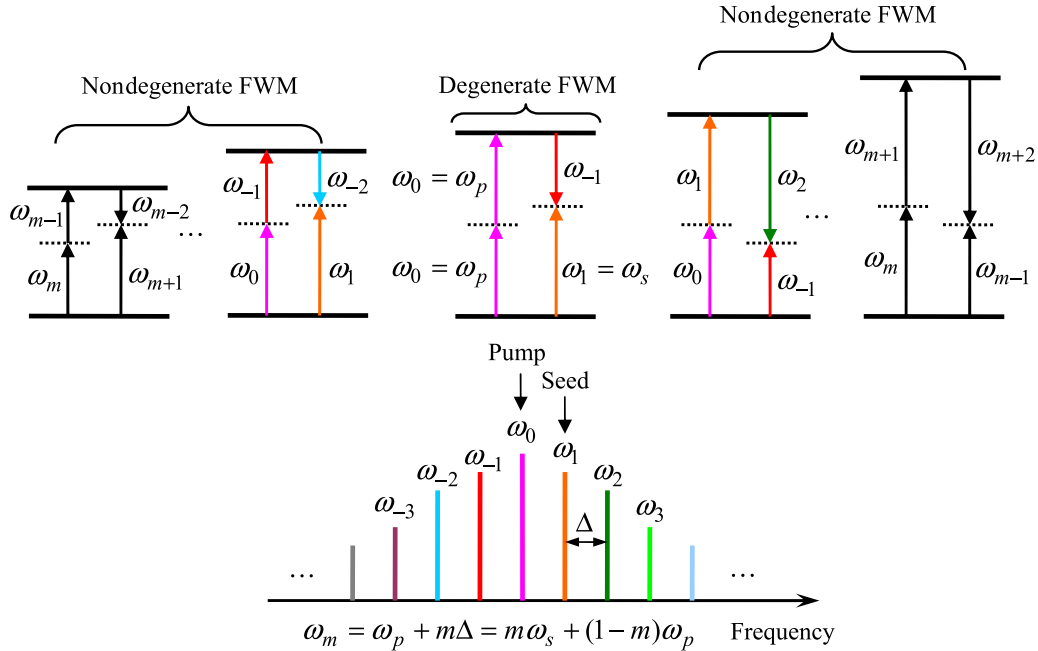


FIG. 4. Energy-level diagram of degenerate and nondegenerate FWM processes. The OFC spectra are generated by a combination of degenerate FWM, in which two identical pump photons at frequency ω_p and a seed photon at frequency ω_s are converted into an idler photon at frequency ω_{-1} , as well as nondegenerate FWM, in which three pump photons at different frequencies ω_{m-1} , ω_m , and ω_{m+1} are converted into a new photon at frequency ω_{m-2} (top left) or ω_{m+2} (top right). The FWM process results in equidistant sidebands. Note that, in the case of CQED-based OFC spectra, the sideband order 0 is the pump field and the sideband order 1 is the seed field.

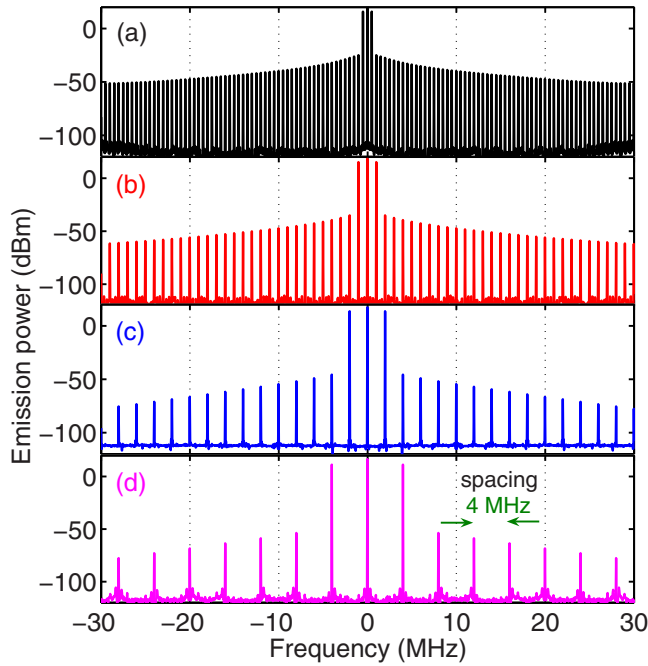


FIG. 5. The OFC spectra generated in the cavity EIT system for four different values of the beating frequency Δ at $\Omega_c/2\pi = 8$ MHz: (a) $\Delta/2\pi = 0.5$ MHz, (b) $\Delta/2\pi = 1$ MHz, (c) $\Delta/2\pi = 2$ MHz, and (d) $\Delta/2\pi = 4$ MHz. The other parameters are the same as in Fig. 2.

a cavity mode, can coherently excite parametric four-wave-mixing (FWM) processes via the atom-cavity-induced strong Kerr nonlinearity [49,50]. There are dominantly two types of FWM, degenerate and nondegenerate, which are clearly illustrated in Fig. 4. First, due to the momentum conservation among the interacting photons, a degenerate FWM process converts two identical pump photons at frequency ω_p and a seed photon at frequency ω_s into an idler photon at frequency ω_{-1} . Then a nondegenerate FWM process converts three pump photons at different frequencies ω_{m-1} , ω_m , and ω_{m+1} , into a new photon at frequency ω_{m-2} or ω_{m+2} . The iteration of these processes thus produces a series of optical high-order comb teeth at frequency $\omega_m = \omega_p + m\Delta = m\omega_s + (1-m)\omega_p$, i.e., the so-called OFCs. Obviously the frequency spacing of the comb teeth is the beating frequency, i.e., the difference Δ in the frequencies of the pump and seed driving fields. As a result, the comb spacing can be finely tuned by setting Δ . Finally, by means of the uncertainty relations of time and energy [51], it is easy to calculate the uncertainty of the frequency as $\Delta\omega = \Delta E/\hbar \sim 2\pi/\tau$. The applied biharmonic driving (see Fig. 1) is two cw lasers and lasts about infinity, i.e., $\tau \rightarrow +\infty$. In this case, we can obtain the comb-tooth linewidth $\Delta\omega \rightarrow 0$ in the frequency domain as shown in Fig. 2. Thus the comb teeth are relatively narrow sharp sideband lines.

In order to further check whether the comb spacing can be tuned by setting the frequency difference Δ between the pump and seed fields, we proceed to examine the OFC generation with a numerical simulation to vary the frequency difference Δ . In Fig. 5 we plot the OFC spectra under the same conditions as in Fig. 2(c), but with four different values of the frequency difference Δ . It is clearly shown in Fig. 5 that tunable comb spacings of $2\pi \times 0.5$, $2\pi \times 1$, $2\pi \times 2$, and $2\pi \times 4$ MHz

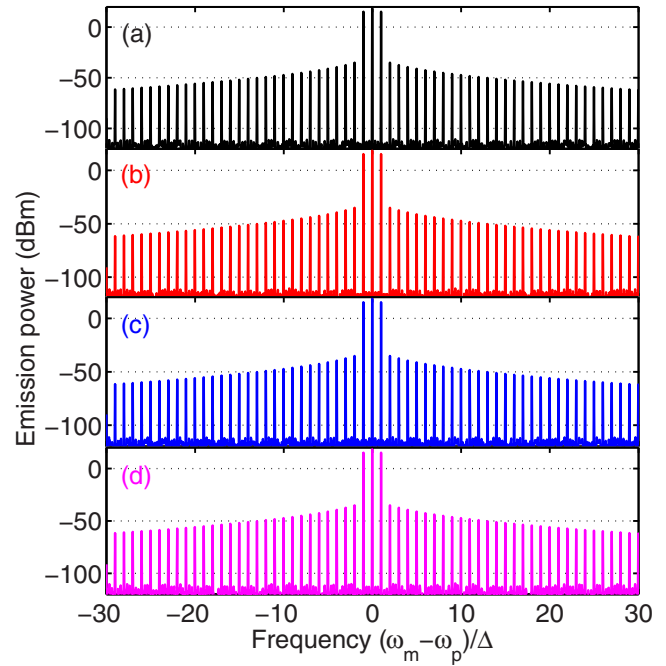


FIG. 6. The OFC spectra generated in the cavity EIT system for four different values of the phase noise ϕ at $\Omega_c/2\pi = 8$ MHz: (a) $\phi = 0$, (b) $\phi = \pi/4$, (c) $\phi = \pi/2$, and (d) $\phi = 3\pi/4$. The other parameters are the same as in Fig. 2.

for the output spectrum as an example within the frequency bandwidth of $2\pi \times 60$ MHz can be achieved. Specifically, when the frequency difference Δ between the driving pump and seed fields is set as $\Delta/2\pi = 0.5$ MHz in Fig. 5(a), the OFC is generated with 120 comb lines within the given frequency bandwidth of $2\pi \times 60$ MHz. For the case of $\Delta/2\pi = 1$ MHz in Fig. 5(b), the number of comb lines is decreased to the value of 60, which is half as many as in Fig. 5(a). For the case of $\Delta/2\pi = 2$ MHz in Fig. 5(c), there are 30 comb lines. Further increasing $\Delta/2\pi = 4$ MHz in Fig. 5(d), only 15 bars of comb lines occur. Moreover, via numerical estimations it is predicted that the lower limit of the repetition rate is taken to be $\Delta/2\pi \sim 0.1$ MHz and the upper limit is taken to be $\Delta/2\pi \sim 10$ MHz. Overall, a closer view of Fig. 5 reveals that the quantity Δ indeed plays an important role in the amount of comb spacing. Furthermore, we also confirm that the comb spacing is directly determined by the frequency difference Δ between the driving pump and seed fields.

The stability of the OFC repetition frequency is determined by the stability of the beat frequency Δ . Therefore, at this stage, one may ask the following question: Does the phase noise in the beat frequency Δ influence the generation of the OFC? To answer this question, the biharmonic driving laser (i.e., pump plus seed) needs to be rewritten in the form $S_{\text{dri}}(t) = \mathcal{E}_p + \mathcal{E}_s e^{-i\Delta t + i\phi}$ in the rotating frame at ω_c , where ϕ stands for the known phase noise from the beating frequency Δ . In Fig. 6 we present the OFC spectra by adding four different values of the phase noise under the same conditions as in Fig. 2(c). As can be seen from Fig. 6, also including the other phase noise values (not shown here), the frequency of the certain comb line is stable, which is independent of the change in the phase noise ϕ . Of course, the stability of the phase noise spectrum is also superb.

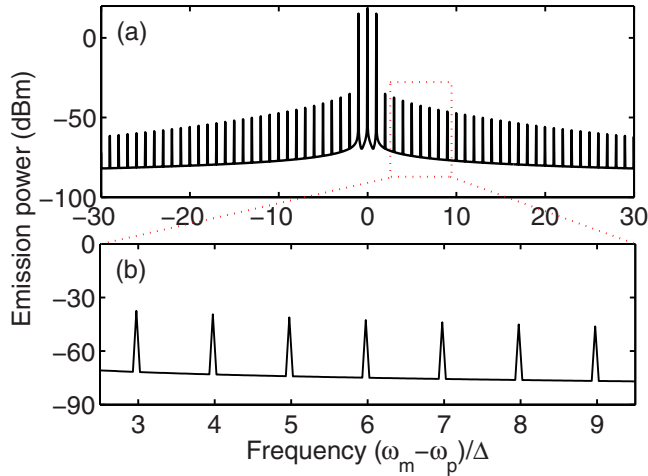


FIG. 7. (a) The OFC spectra generated in the cavity EIT system when we set, in our model, the duration of the pump, seed, and control lasers equal to $\tau_s = 50$ ms. (b) Magnified view of the OFC spectrum from (a) in a smaller region. The other parameters are the same as in Fig. 2.

Finally, it is important to mention that, in the above analysis, we have neglected the linewidth of the pump, seed, and control lasers. A natural question to ask, then, is how the laser linewidth influences the linewidth of the comb tooth. To properly address this problem we start from a nonzero linewidth for the applied lasers via a numerical simulation. The detailed result for the OFC spectrum is displayed in Fig. 7. From this figure it can be found that there are certain widths of the OFC spectral features. Concretely, we model the signal driving laser involved here as a Gaussian-shaped wave packet in Fig. 7, where the total duration is about $\Delta t = 2\tau_s \sim 100$ ms. According to the basic theory of the uncertainty relations mentioned above, it is straightforward to preliminarily calculate the linewidth of the comb tooth as $\Delta\omega/2\pi \sim 0.01$ kHz in the frequency regime.

As a consequence, the generated OFC spectrum is still robust in the presence of the laser linewidth.

IV. CONCLUSION

We have demonstrated theoretically that by means of a single three-level Λ -type atom in a high-finesse cavity it is possible to generate and optically control OFCs via a combination of EIT and single-atom CQED. The generated OFCs can be largely enhanced or suppressed, depending on the control-laser parameters. Also, a few-megahertz repetition rate can be obtained in our scheme, which is small for any microcomb. We discuss the properties of the intracavity dark mode and indicate that the formation of the dark mode enables the efficient generation of OFCs in this cavity EIT system. Recent experiments [18,19,21] have provided the feasibility of the proposal and the presented mechanism can be employed to tailor and control OFCs in a CQED architecture. We believe that our proposal is feasible in experimental realizations and deserves to be tested with currently available technology.

ACKNOWLEDGMENTS

We thank the two anonymous referees for their valuable suggestions, which significantly improved our paper. We also acknowledge our helpful discussions with Professor Xiaoxue Yang at School of Physics, Huazhong University of Science and Technology in the manuscript preparation. J.L. and Y.Q. are supported by the National Natural Science Foundation of China under Grant No. 11675058. R.Y. is supported by the National Natural Science Foundation of China under Grant No. 11505131 and the Youth Fund Project of Wuhan Institute of Technology under Grant No. Q201408. Y.W. is supported in part by the National Key Research and Development Program of China under Grant No. 2016YFA0301200 and the National Natural Science Foundation of China under Grant No. 11574104.

-
- [1] S. T. Cundiff and J. Ye, Colloquium: Femtosecond optical frequency combs, *Rev. Mod. Phys.* **75**, 325 (2003).
 - [2] T. Udem, R. Holzwarth, and T. W. Hänsch, Optical frequency metrology, *Nature (London)* **416**, 233 (2002).
 - [3] T. J. Kippenberg, R. Holzwarth, and S. A. Diddams, Microresonator-based optical frequency combs, *Science* **332**, 555 (2011).
 - [4] P. Del'Haye, A. Schliesser, O. Arcizet, T. Wilken, R. Holzwarth, and T. J. Kippenberg, Optical frequency comb generation from a monolithic microresonator, *Nature (London)* **450**, 1214 (2007).
 - [5] J. Li, H. Lee, T. Chen, and K. J. Vahala, Low-Pump-Power, Low-Phase-Noise, and Microwave to Millimeter-Wave Repetition Rate Operation in Microcombs, *Phys. Rev. Lett.* **109**, 233901 (2012).
 - [6] J. Li, R. Yu, and Y. Wu, Dipole-induced high-order sideband comb employing a quantum dot strongly coupled to a photonic crystal cavity via a waveguide, *Phys. Rev. B* **89**, 035311 (2014).
 - [7] J. Li, R. Yu, J. Ma, and Y. Wu, All-optical control of optical frequency combs via quantum interference effects in a single-emitter-microcavity system, *Phys. Rev. A* **91**, 063834 (2015).
 - [8] S. E. Harris, Electromagnetically induced transparency, *Phys. Today* **50** (7), 36 (1997).
 - [9] M. Xiao, Y. Q. Li, S. Z. Jin, and J. Gea-Banacloche, Measurement of Dispersive Properties of Electromagnetically Induced Transparency in Rubidium Atoms, *Phys. Rev. Lett.* **74**, 666 (1995).
 - [10] M. Fleischhauer, A. Imamoglu, and J. P. Marangos, Electromagnetically induced transparency: Optics in coherent media, *Rev. Mod. Phys.* **77**, 633 (2005).
 - [11] Y. Wu and X. X. Yang, Electromagnetically induced transparency in V-, Λ -, and cascade-type schemes beyond steady-state analysis, *Phys. Rev. A* **71**, 053806 (2005).
 - [12] L. V. Hau, S. E. Harris, Z. Dutton, and C. H. Behroozi, Light speed reduction to 17 metres per second in an ultracold atomic gas, *Nature (London)* **397**, 594 (1999).

- [13] D. F. Phillips, A. Fleischhauer, A. Mair, R. L. Walsworth, and M. D. Lukin, Storage of Light in Atomic Vapor, *Phys. Rev. Lett.* **86**, 783 (2001).
- [14] Y. Wu and L. Deng, Ultra slow bright and dark optical solitons in a cold three-state medium, *Opt. Lett.* **29**, 2064 (2004).
- [15] L. Slodička, G. Hétet, S. Gerber, M. Hennrich, and R. Blatt, Electromagnetically Induced Transparency from a Single Atom in Free Space, *Phys. Rev. Lett.* **105**, 153604 (2010).
- [16] W. R. Kelly, Z. Dutton, J. Schlafer, B. Mookerji, T. A. Ohki, J. S. Kline, and D. P. Pappas, Direct Observation of Coherent Population Trapping in a Superconducting Artificial Atom, *Phys. Rev. Lett.* **104**, 163601 (2010).
- [17] A. A. Abdumalikov, Jr., O. Astafiev, A. M. Zagoskin, Y. A. Pashkin, Y. Nakamura, and J. S. Tsai, Electromagnetically Induced Transparency on a Single Artificial Atom, *Phys. Rev. Lett.* **104**, 193601 (2010).
- [18] J. McKeever, A. Boca, A. D. Boozer, R. Miller, J. R. Buck, A. Kuzmich, and H. J. Kimble, Deterministic generation of single photons from one atom trapped in a cavity, *Science* **303**, 1992 (2004).
- [19] T. Wilk, S. C. Webster, A. Kuhn, and G. Rempe, Single-atom single-photon quantum interface, *Science* **317**, 488 (2007).
- [20] I. Schuster, A. Kubanek, A. Fuhrmanek, T. Puppe, P. W. H. Pinkse, K. Murr, and G. Rempe, Nonlinear spectroscopy of photons bound to one atom, *Nat. Phys.* **4**, 382 (2008).
- [21] A. Reiserer, N. Kalb, G. Rempe, and S. Ritter, A quantum gate between a flying optical photon and a single trapped atom, *Nature (London)* **508**, 237 (2014).
- [22] M. Keller, B. Lange, K. Hayasaka, W. Lange, and H. Walther, Continuous generation of single photons with controlled waveform in an ion-trap cavity system, *Nature (London)* **431**, 1075 (2004).
- [23] M. Steiner, H. M. Meyer, J. Reichel, and M. Köhl, Photon Emission and Absorption of a Single Ion Coupled to an Optical-Fiber Cavity, *Phys. Rev. Lett.* **113**, 263003 (2014).
- [24] R. Reimann, Cooling and cooperative coupling of single atoms in an optical cavity, Ph.D. thesis, Universität Bonn, 2014, available at <https://hss.ulb.uni-bonn.de/2014/3832/3832.pdf>.
- [25] M. Albert, A. Dantan, and M. Drewsen, Cavity electromagnetically induced transparency and all-optical switching using ion Coulomb crystals, *Nat. Photon.* **5**, 633 (2011).
- [26] A. Reiserer and G. Rempe, Cavity-based quantum networks with single atoms and optical photons, *Rev. Mod. Phys.* **87**, 1379 (2015).
- [27] A. D. Boozer, A. Boca, R. Miller, T. E. Northup, and H. J. Kimble, Reversible State Transfer Between Light and a Single Trapped Atom, *Phys. Rev. Lett.* **98**, 193601 (2007).
- [28] M. Mücke, E. Figueroa, J. Bochmann, C. Hahn, K. Murr, S. Ritter, C. J. Villas-Boas, and G. Rempe, Electromagnetically induced transparency with single atoms in a cavity, *Nature (London)* **465**, 755 (2010).
- [29] T. Kampschulte, W. Alt, S. Brakhane, M. Eckstein, R. Reimann, A. Widera, and D. Meschede, Optical Control of the Refractive Index of a Single Atom, *Phys. Rev. Lett.* **105**, 153603 (2010).
- [30] M. Bienert and G. Morigi, Cavity cooling of a trapped atom using electromagnetically induced transparency, *New J. Phys.* **14**, 023002 (2012).
- [31] J. A. Souza, E. Figueroa, H. Chibani, C. J. Villas-Boas, and G. Rempe, Coherent Control of Quantum Fluctuations Using Cavity Electromagnetically Induced Transparency, *Phys. Rev. Lett.* **111**, 113602 (2013).
- [32] T. Kampschulte, W. Alt, S. Manz, M. Martinez-Dorantes, R. Reimann, S. Yoon, D. Meschede, M. Bienert, and G. Morigi, Electromagnetically-induced-transparency control of single-atom motion in an optical cavity, *Phys. Rev. A* **89**, 033404 (2014).
- [33] H. S. Borges and C. J. Villas-Boas, Quantum PHASE gate based on electromagnetically induced transparency in optical cavities, *Phys. Rev. A* **94**, 052337 (2016).
- [34] J. Sheng, Y. Chao, S. Kumar, H. Fan, J. Sedlacek, and J. P. Shaffer, Intracavity Rydberg-atom electromagnetically induced transparency using a high-finesse optical cavity, *Phys. Rev. A* **96**, 033813 (2017).
- [35] R. R. Oliveira, H. S. Borges, J. A. Souza, and C. J. Villas-Boas, Quantum memory and optical transistor based on electromagnetically induced transparency in optical cavities, [arXiv:1603.05127v1](https://arxiv.org/abs/1603.05127v1).
- [36] K. J. Vahala, Optical microcavities, *Nature (London)* **424**, 839 (2003).
- [37] H. J. Kimble, The quantum internet, *Nature (London)* **453**, 1023 (2008).
- [38] H. J. Kimble, Strong interactions of single atoms and photons in cavity QED, *Phys. Scr.* **T76**, 127 (1998).
- [39] P. G. Westergaard, B. T. R. Christensen, D. Tieri, R. Matin, J. Cooper, M. Holland, J. Ye, and J. W. Thomsen, Observation of Motion-Dependent Nonlinear Dispersion with Narrow-Linewidth Atoms in an Optical Cavity, *Phys. Rev. Lett.* **114**, 093002 (2015).
- [40] Y. D. Kwon, M. A. Armen, and H. Mabuchi, Femtojoule-Scale All-Optical Latching and Modulation via Cavity Nonlinear Optics, *Phys. Rev. Lett.* **111**, 203002 (2013).
- [41] P. E. Barclay, K. M. C. Fu, C. Santori, and R. G. Beausoleil, Chip-based microcavities coupled to nitrogen-vacancy centers in single crystal diamond, *Appl. Phys. Lett.* **95**, 191115 (2009).
- [42] A. Badolato, K. Hennessy, M. Atatüre, J. Dreiser, E. Hu, P. M. Petroff, and A. Imamoglu, Deterministic coupling of single quantum dots to single nanocavity modes, *Science* **308**, 1158 (2005).
- [43] M. Pelton, C. Santori, J. Vucković, B. Zhang, G. S. Solomon, J. Plant, and Y. Yamamoto, Efficient Source of Single Photons: A Single Quantum Dot in a Micropost Microcavity, *Phys. Rev. Lett.* **89**, 233602 (2002).
- [44] A. Wallraff, D. I. Schuster, A. Blais, L. Frunzio, R.-S. Huang, J. Majer, S. Kumar, S. M. Girvin, and R. J. Schoelkopf, Strong coupling of a single photon to a superconducting qubit using circuit quantum electrodynamics, *Nature (London)* **431**, 162 (2004).
- [45] J. Q. You and F. Nori, Atomic physics and quantum optics using superconducting circuits, *Nature (London)* **474**, 589 (2011).
- [46] E. Waks and D. Sridharan, Cavity QED treatment of interactions between a metal nanoparticle and a dipole emitter, *Phys. Rev. A* **82**, 043845 (2010).
- [47] Y.-C. Liu, Y.-F. Xiao, B.-B. Li, X.-F. Jiang, Y. Li, and Q. Gong, Coupling of a single diamond nanocrystal to a whispering-gallery microcavity: Photon transport benefit-

- ting from Rayleigh scattering, [Phys. Rev. A **84**, 011805\(R\) \(2011\)](#).
- [48] C. Dong, V. Fiore, M. C. Kuzyk, and H. Wang, Optomechanical dark mode, [Science **338**, 1609 \(2012\)](#).
- [49] Y. F. Zhu, Large Kerr nonlinearities on cavity-atom polaritons, [Opt. Lett. **35**, 303 \(2010\)](#).
- [50] J. Li, S. Zhang, R. Yu, D. Zhang, and Y. Wu, Enhanced optical nonlinearity and fiber-optical frequency comb controlled by a single atom in a whispering-gallery-mode microtoroid resonator, [Phys. Rev. A **90**, 053832 \(2014\)](#).
- [51] A. Messiah, *Quantum Mechanics* (North-Holland, Amsterdam, 1965), Vol. 2.